POLITECNICO DI TORINO
Repository ISTITUZIONALE

Assessing arterial wave transmission from micro- to hypergravity: A multiscale cardiovascular modeling approach

Original
Assessing arterial wave transmission from micro- to hypergravity: A multiscale cardiovascular modeling approach / Scarsoglio, S., Colussi, G., Tripoli, F., Ridolfi, L.. - In: PHYSICS OF FLUIDS. - ISSN 1070-6631. - 38:8(2026). [10.1063/5.0334204]

Availability:
This version is available at: 11583/3016870 since: 2026-10-22T08:50:42Z

Publisher:
AIP Publishing

Published
DOI:10.1063/5.0334204

Terms of use:

This article is made available under terms and conditions as specified in the corresponding bibliographic description in the repository

Publisher copyright

(Article begins on next page)

26 November 2026

Physics of Fluids

RESEARCH ARTICLE | AUGUST 18 2026

Assessing arterial wave transmission from micro- to hypergravity: A multiscale cardiovascular modeling approach

S. Scarsoglio ; G. Colussi ; F. Tripoli ; L. Ridolfi

Check for updates

Physics of Fluids 38, 081910 (2026)
https://doi.org/10.1063/5.0334204

View Online
Export Citation

Articles You May Be Interested In

Coupling the rheology of blood samples with low and high cholesterol levels to a one-dimensional cardiovascular formulation

Physics of Fluids (May 2026)

An advanced immersed fluid–structure interaction particle method for cardiovascular applications experimentally validated vs a new benchmark case

Physics of Fluids (March 2026)

Hemodynamics of slip surfaces for thrombosis control in implanted cardiovascular devices

Physics of Fluids (February 2025)

23 October 2026 06:47:30

AIP Publishing

Physics of Fluids

Special Topics Open for Submissions

Learn More

AIP Publishing

Physics of Fluids ARTICLE pubs.aip.org/aip/pof

Assessing arterial wave transmission from micro- to hypergravity: A multiscale cardiovascular modeling approach

Cite as: Phys. Fluids **38**, 081910 (2026); doi: 10.1063/5.0334204
Submitted: 17 March 2026 · Accepted: 29 July 2026 ·
Published Online: 18 August 2026

View Online Export Citation CrossMark

S. Scarsoglio,[1,2,a)] G. Colussi,[1] F. Tripoli,[1] and L. Ridolfi[2,3]

AFFILIATIONS

[1]Department of Mechanical and Aerospace Engineering, Politecnico di Torino, Corso Duca degli Abruzzi 24, Torino 10129, Italy
[2]PolitoBioMed Lab, Politecnico di Torino, Corso Duca degli Abruzzi 24, Torino 10129, Italy
[3]Department of Environmental, Land and Infrastructure Engineering, Politecnico di Torino, Corso Duca degli Abruzzi 24, Torino 10129, Italy

[a)]**Author to whom correspondence should be addressed:** stefania.scarsoglio@polito.it

ABSTRACT

The human cardiovascular system is adapted to terrestrial gravity, yet transitions toward microgravity and hypergravity induce marked blood redistribution and hemodynamic changes. Despite their clinical relevance, arterial pressure and flow wave dynamics under altered gravity remain poorly characterized, owing to scarce direct measurements beyond ground-based studies. Here, a validated fluid dynamics-based multiscale cardiovascular model was used to investigate arterial wave transmission and reflection in standing posture across the $0g$–$3g$ range. Pulse wave velocity maintained its proximal-to-distal increase at fixed g, while showing opposite gravity-dependent trends across the orthostatic indifference point (decreasing above and increasing below), mainly driven by wall stiffness changes. Backward waves were attenuated more than forward waves, and reflection indices decreased throughout the network, including the lower limbs. Bifurcation- and tapering-related effects were only weakly gravity-sensitive, whereas distal peripheral resistances emerged as the dominant mechanism modulating wave amplitudes. Wave trapping remained preserved along the aortic tract, limiting central reflected wave load. Present findings indicate a gravity-resilient wave-filtering behavior of the arterial network and provide a mechanistic framework for studying cardiovascular adaptation to extreme environments.

© 2026 Author(s). All article content, except where otherwise noted, is licensed under a Creative Commons Attribution (CC BY) license (https://creativecommons.org/licenses/by/4.0/). https://doi.org/10.1063/5.0334204

23 October 2026 06:47:30

I. INTRODUCTION

The human cardiovascular system has evolved based on terrestrial gravity. It follows that variations in gravitational or postural loading, either during micro- or hypergravity exposure (e.g., spaceflight and centrifugation) or in terrestrial pathological conditions (e.g., bedridden states and dysautonomia), induce a constellation of alterations ranging from increased cerebral pressure and cardiac preload to orthostatic hypotension, venous pooling, and reduced venous return.[1–4] All these hemodynamic changes are first driven and ruled by fluid dynamics processes, starting from the blood shift in the caudal (hypergravity) or cranial (microgravity) directions, and then partially mitigated by the autonomic vascular and cardiac control mechanisms. Although the overall picture of gravity-induced hemodynamic changes is fairly well established, the inherent challenges of obtaining clinical measurements in extreme environments and pathological conditions limit the characterization of the cardiovascular response to a restricted set of conventional cardiac parameters [e.g., heart rate (*HR*), stroke volume (*SV*), and arterial blood pressure]. In particular, although the dynamics of arterial pressure and flow waves are key indicators of cardiovascular function,[5–9] they remain poorly studied under altered gravity conditions (from micro- to hypergravity) and constitute the focus of the present study.

Arterial pressure and flow waves are generated at the aortic root by the rhythmic contraction and relaxation of the left ventricle. As these waves pass through the aortic valve and move through successive bifurcations into peripheral branches, they encounter geometrical and mechanical changes that create continuous reflection, namely backward waves.[10–13] Thus, local pressure and flow waveforms are the result of the superposition of forward and backward components, arising from a complex interplay among vascular topology and wall

© Author(s) 2026

properties, peripheral reflections, cardiac forcing, autoregulation, posture as well as gravity changes.

At terrestrial gravity, supine wave transmission and reflection studies have mainly focused on pulse wave velocity (PWV) along major arterial paths,[14,15] with PWV being a standard marker of arterial stiffness and vascular aging.[16,17] Previous studies consistently observe a PWV increase from proximal to peripheral regions, primarily driven by reduced compliance, augmented stiffness, and tapering vessel diameters.[6,10,13] Furthermore, the phenomenon of wave trapping emerges. This is defined as a physiological mechanism that sequesters most of the reflected wave energy within the peripheral vasculature, thereby providing natural protection for the heart by minimizing the return of backward traveling waves to the aortic root.[18–20] However, orthostatic effects (supine-to-upright) are less characterized. *In vivo* studies indicate reduced wave reflections during upright tilt despite increased peripheral resistance and PWV,[21–24] in agreement with our computational finding of preserved wave trapping across postural transitions.[25]

While few studies have examined postural effects on wave transmission at terrestrial gravity, to the best of our knowledge there are no direct measurements or computational analyses across gravity levels (from microgravity to hypergravity) in upright posture. Human spaceflight data are essentially limited to pre- and post-flight assessments.[26,27] Terrestrial analogs (e.g., water immersion, head-down bed rest, parabolic flights, and centrifuges) can partially reproduce altered gravity conditions. However, available evidence is mostly limited to microgravity analogs and long-term effects,[28–33] whereas hypergravity data remain scarce, as parabolic and centrifuge experiments are technically demanding even for noninvasive measurements.

To fill these gaps, we computationally investigate arterial wave propagation in standing posture across 0*g*–3*g*, and analyze how gravity reshapes pressure/flow waveforms through coupled mechanical, geometrical, and autoregulatory effects. Specifically, we quantify changes in wave transmission and reflection from microgravity (0*g*), through hypogravity (0*g*–1*g*), to hypergravity (1*g*–3*g*). We adopt a validated fluid-dynamics-based multiscale 0D–1D cardiovascular model, consistent with current applications of multiscale hemodynamic modeling beyond resting conditions.[34–36] This framework has been previously validated and used to investigate postural effects,[37,38] gravity-related hemodynamics,[39–41] and cardiovascular pathologies such as cardiac arrhythmias.[42–45] Waveform analysis is performed at multiple arterial sites. After PWV estimation and wave decomposition, forward and backward pressure/flow components are evaluated through reflection indices. We then assess the contributions of geometrical and mechano-structural factors (diameter, thickness, bifurcations, tapering) and distal compliance/absorption, and finally test whether wave trapping from the aortic root to tibial arteries remains a protective barrier across gravity levels.

II. METHODS

We adopt a previously validated multiscale cardiovascular model combining a 1D representation of the large systemic and coronary arteries with lumped-parameter (0D) models of the remaining circulation, including distal vascular beds, venous return, cardiopulmonary circulation, and cerebro-ocular districts. At terminal sites, 1D arteries are coupled to 0D arteriolar beds through pressure–flow boundary conditions, combining the downstream lumped-parameter load with the compatibility relation from the 1D arterial domain. The framework incorporates short-term physiological control (baroreflex, cardiopulmonary reflex, and cerebral autoregulation), venous collapse, and the explicit body-force effects due to gravity and posture changes.

Focusing on the large 1D vessels of the systemic circulation, waveform analysis targets pulse wave velocity, c, and the decomposition of pressure, P, and flow rate, Q, waves through the local characteristic impedance, Z_c. In particular, local pulse wave velocity, c, was estimated from the pressure–velocity (PU) loop and used to separate wave intensity into forward and backward components, while the characteristic impedance, Z_c, used for pressure/flow decomposition was obtained from the pressure–flow rate (PQ) loop,[7,9] as detailed in Fig. SM3 of the supplementary material. After separating waves into forward (f) and backward (b) components, transmission and reflection are quantified using standard metrics, namely reflection index (RI) and reflection magnitude (RM), computed from forward/backward wave amplitudes.[25]

To distinguish reflection mechanisms, we evaluate (i) bifurcation-related reflection from local impedance mismatch between parent and daughter branches, through pressure reflection coefficients, R_p, in forward and backward directions; (ii) tapering-related reflection from progressive axial impedance variation within each vessel segment, quantified by R_t; and (iii) terminal branch reflection from distal boundary impedance at network outlets, expressed by the ratio r between the gravity-induced variation of the backward wave and that of the associated forward wave. This decomposition isolates the relative roles of geometry (branching and tapering) and distal loading (terminal beds) in shaping total reflected wave content under altered gravity.

We also evaluate the time of reflection (ToR) as $ToR = t_{back} - t_{fcw}$, where t_{fcw} is the arrival time of the first forward compression wave and t_{back} is the intensity-weighted centroid of the backward wave-intensity signal. This centroid-based definition is appropriate because backward waves arise from multiple distributed reflections and partially overlap owing to wave trapping and horizon effects,[18,25] making the selection of a unique backward wave onset difficult and threshold-dependent. ToR is introduced to quantify reflected wave return timing and, therefore, to assess wave trapping efficiency along the arterial tree: longer ToR and delayed backward wave return are consistent with stronger peripheral trapping by vessel network and reduced central reflected wave load.

Full model structure, governing equations, parameter values, boundary conditions, numerical implementation, as well as a complete and formal description of the adopted waveform analysis framework are provided in the supplementary material.

III. RESULTS

Waveform analysis in the range [0*g*, 3*g*] was performed with incremental steps of 0.1*g* and at different arterial sites (nomenclature reported in the supplementary material): the right internal carotid artery (ICA) (No. 12), the right external carotid artery (No. 13), the aortic root (No. 1), the aortic arch (No. 2), the first thoracic aortic segment (No. 18), the second thoracic aortic segment (No. 27), the third abdominal aortic segment (No. 37), the common iliac artery (No. 42), the external iliac artery (No. 44), the femoral artery (No. 46), and the anterior tibial artery (No. 47). Before presenting model-based wave transmission results, we here summarize some key trends as a

23 October 2026 06:47:30

© Author(s) 2026

function of g validated against available clinical literature,[39,40] that support interpretation of Secs. III A–III D.

Ranging from 0g to 3g, blood volume shifts toward the lower body, away from both the central region—reflected by reductions in stroke volume, SV (0g: 82.9 ml; 3g: 32.5 ml), and central venous pressure, CVP (0g: 6.6 mm Hg; 3g: −1 mm Hg)—and the cranial compartment—evidenced by decreases in intracranial pressure, ICP (0g: 10.1 mm Hg; 3g: −8.9 mm Hg) and cerebral blood flow, CBF (0g: 12.4 ml/s; 3g: 7.5 ml/s). These significant changes occur despite the fact that short-term regulatory mechanisms act to limit excessive pooling and orthostatic hypotension. Among these compensatory responses, the most consistently observed is an increase in heart rate, HR (0g: 66 bpm; 3g: 128 bpm), which partially counteracts SV reduction and helps maintain adequate cardiac output, $CO = SV \times HR$ (0g: 5.45 l/min; 3g: 4.16 l/min), and mean central aortic pressure (0g: 92 mm Hg; 3g: 92 mm Hg).

A. Pressure and flow rate waveforms along the arterial tree

Pressure and flow rate waveforms over a cardiac cycle at three representative arterial sites and under four gravitational conditions (0g, 1g, 2g, and 3g) are shown in the left panels of Fig. 1. Some relevant aspects clearly emerge from the analysis of the wave patterns. First, as previously noted, when gravitational acceleration increases, the duration of the cardiac cycle becomes shorter, decreasing from 0.91 s in microgravity to 0.46 s in 3g. Second, as gravity grows, the pulse wave values (i.e., wave amplitudes) progressively decrease at all analyzed sites for both pressure and flow rate, reducing the overall excursion of both variables throughout the cardiac cycle. Third, although pulse values exhibit a common decreasing trend for both pressure and flow rates, the extent of reduction differs along the arterial pathway for the pressure and flow waves. Specifically, while the decrease in pulse pressure is more pronounced in the central region compared to the body periphery, the reduction in flow pulse values becomes progressively more significant with increasing distance from the heart. The percentage decrease in pulse pressures between 0g *and* 3g ranges from −55.6% at the aortic root to −41.3% at the anterior tibial artery. In contrast, the pulsatility of flow rate waves decreases by −31.4% at the aortic root, reaching −48.9% at the iliac artery and −54.0% at the anterior tibial site. In the end, in the lower-body regions, both the minimum and maximum pressure values increase as g increases. In particular, the reduction in pulsatility appears to result from a greater increase in wave-foot values compared to the increase in peak pressure values. In contrast, in the central region, the reduction in pulse pressure is due to both an increase in the wave-foot value and a decrease in the maximum pressure.

Mean pressure values (reported in Table SM11 of the supplementary material) show limited variability in the central region (i.e., aortic root and thoracic aorta), whereas all sites located along the arterial pathway from the abdominal aorta to the anterior tibial artery exhibit progressively increasing mean pressure values as g increases. Furthermore, the percentage increase from 0g to 3g in mean pressure is more pronounced in the peripheral region: in the anterior tibial artery, the percentage variation is approximately +246%, compared to +48.2% at the abdominal aorta and −0.076% at the aortic root. In

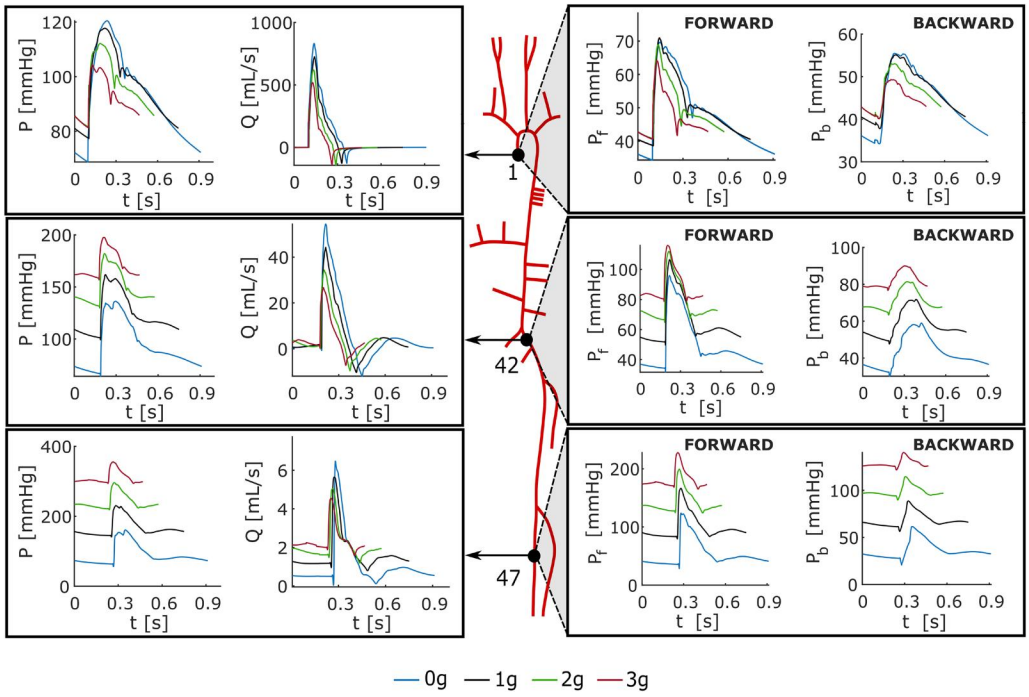

FIG. 1. Temporal wave patterns over an entire cardiac cycle, under four gravitational conditions [0g (blue), 1g (black), 2g (green), and 3g (red)], at three representative arterial sites (marked by black circles): aortic root (No. 1), common iliac artery (No. 42), and anterior tibial artery (No. 47). Left: total pressure (P) and flow rate (Q) waves. Right: forward and backward pressure (P) waves.

23 October 2026 06:47:30

© Author(s) 2026

contrast, sites located above the heart level show a clear decreasing trend in mean pressure values as g increases. For example, the internal carotid artery exhibits a percentage variation from $0g$ to $3g$ of approximately −39.6%. As a consequence of the observed trend in mean pressure, the heart level can be assumed to be a discriminating point in terms of pressure wave alterations when the orthostatic load changes (i.e., the orthostatic indifference point, OIP).

Mean values of flow rate waves exhibit a different trend based on their spatial distribution along the arterial tree. Unlike mean pressure values, the discriminating region appears to be the lower abdominal/iliac area. Specifically, along the entire aortic pathway up to the iliac artery, mean flow rates decrease with increasing gravitational stress. As reported in Table SM11 of the supplementary material, the associated percentage variations between $0g$ *and* $3g$ range from −26.2% (iliac artery) to −35.8% (thoracic aorta). In contrast, mean flow rate values in the lower limbs increase as g increases, with values rising toward the periphery (+80% for the femoral artery and +120% for the anterior tibial artery). As gravitational stress increases, the central and abdominal regions undergo a sort of homogeneous "emptying," leading to reduced mean arterial flow rates, while an opposite "filling" trend is observed in the lower limbs.

B. Pulse wave velocity pattern

The evaluation of the local pulse wave velocity was performed according to the PU-loop method,[9,25] as described in Sec. SM3 of the supplementary material. Figure 2(a) illustrates the resulting trend of c across all arterial sites in the range $[0g, 3g]$. Two distinct trends for c emerge: a spatial trend and a gravity-related one. First, under a fixed gravitational condition, c increases with the distance from the heart. This spatial trend is observed at sites located above the OIP as well as at the aortic and lower-limb sites, and is preserved across the entire gravity range analyzed. Second, c values show clear trends with respect to gravitational stress at fixed arterial locations. In vessels located above heart level, a progressive decrease in c is observed, whereas below the OIP wave velocity exhibits an overall increasing trend with increasing g. Moreover, the decrease/increase becomes more pronounced as the distance from the heart increases.

The Moens–Korteweg relation[46] enabled us to understand the mechanisms underlying the observed trends of c. It reads

$$c = \sqrt{\frac{hE}{\rho d}} = \sqrt{\frac{A}{\rho C_A}}, \tag{1}$$

where h is the wall vessel thickness, E is the wall stiffness, ρ is the blood density, d is the internal diameter, A is the vessel cross-sectional area, and C_A is the area compliance. Notice that the validity of Eq. (1) is constrained by the assumption of linear elastic behavior of the vessel walls. Instead, the material composing arterial walls exhibits both elastic and viscous characteristics, leading to a time-dependent stress–strain response. Moreover, biological tissues display nonlinear elasticity, so the stress-dependent Young's modulus is assumed to be given by the local tangent to the stress–strain curve (i.e., $E = E_{inc}$, where E_{inc} is the incremental elastic modulus). Therefore, we used the relation not for direct quantitative predictions but rather as a conceptual reference to interpret how different parameters influence c.

According to Eq. (1), c depends on three factors: fluid compressibility (assumed negligible here, as blood is considered an incompressible fluid), vessel geometric properties (d and h), and wall mechanical properties (E_{inc}). Concerning the spatial trend of c, the analysis of the

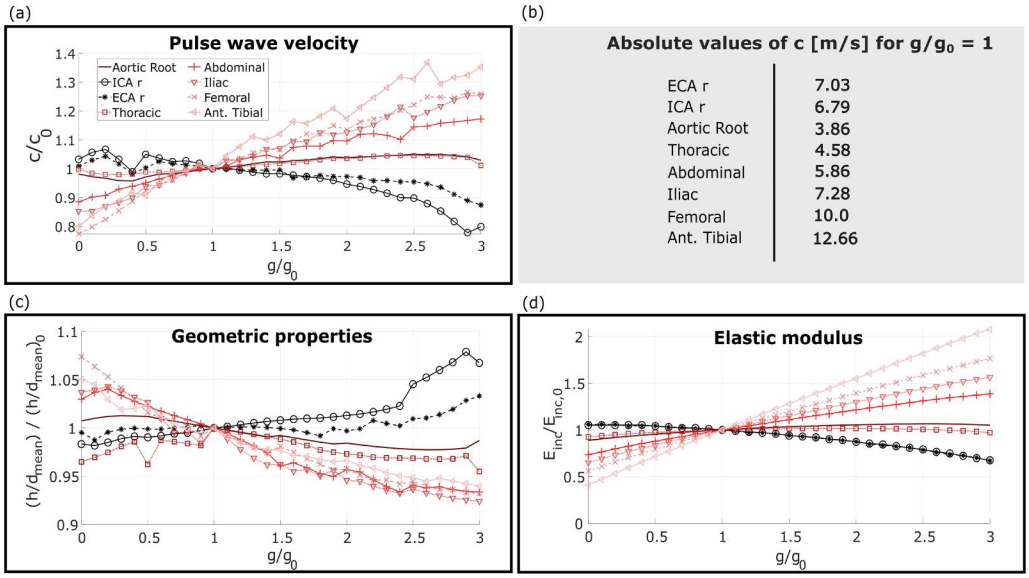

FIG. 2. Variation of pulse wave velocity and its governing factors as a function of gravity level. (a) Pulse wave velocity c at the analyzed arterial locations (nos. 1, 12, 13, 18, 37, 42, 46, 47) across the gravitational range $0g$–$3g$. Values are normalized with respect to the baseline value of c_0 at $1g$. Red lines refer to the vessels located in the central and lower body region, while black lines refer to the vessels positioned in the upper body (i.e., internal and external carotid arteries). (b) Absolute values of c of the baseline case, $1g$. (c) Ratio between arterial wall thickness h and mean lumen diameter d_{mean} at the same locations as a function of the gravity level; values are normalized with respect to the corresponding baseline values at $1g$. (d) Young's modulus E_{inc} at the same locations as a function of the gravity level, normalized with respect to the baseline value of $E_{inc,0}$ at $1g$.

23 October 2026 06:47:30

© Author(s) 2026

vessels' geometric properties along the arterial tree provides a first key for interpreting the obtained results. As illustrated in Fig. SM6 of the supplementary material, both the vessel-averaged internal diameters d_{mean} and wall thickness h physiologically decrease as the distance from the heart increases. However, mean diameters decrease by an order of magnitude more than wall thickness. Consequently, the ratio h/d_{mean} increases with increasing distance from the heart [see Fig. 2(c)], thereby explaining the rise in c along the arterial tree, a behavior that remains consistent across all gravity levels. However, the dependence of h/d_{mean} on gravity is opposite to that shown by the local pulse velocity [compare Figs. 2(a) and 2(c)]: as gravity increases, h/d_{mean} decreases for the arterial sites located below the heart; conversely, c increases (vice versa above the heart). It follows that the reason for the gravity-induced change of c cannot lie in the geometric behavior of the vessels, but must instead arise from the other term of the Moens–Korteweg relation: the mechanical properties of the arterial walls.

The estimation of E_{inc} was obtained from the constitutive P–A relationship (see Sec. SM6 of the supplementary material for more details). Due to the convexity of the stress–strain curve, it is known[47] that E_{inc} increases as the stress applied to the biological material grows. Therefore, Young's modulus varies throughout the cardiac cycle, assuming larger values at pressure peaks (systolic phase) and smaller values at the wave foot (diastolic phase). In Fig. 2(d), we reported E_{inc} values refer to the condition of maximum wall relaxation, i.e., the instant at which the vessel's cross-sectional area is minimal (diastolic phase). However, by selecting other phases of the cardiac cycle for the stiffness analysis, analogous E_{inc} trends would be obtained. It emerges clearly that the effect of gravity on E_{inc} is qualitatively the same as that on celerity c [compare Figs. 2(a) and 2(d)]. The reason is linked to the concavity of the P–A relationship: as gravity load increases, the portion of the arterial tree below (above) the heart (i.e., the OIP) is subject to increasingly greater (lower) average pressures and therefore the cardiac cycle moves along sections of the P–A curve associated with greater (lower) stiffness. Finally, notice that not only does E_{inc} change with g at each site, but the magnitude of this variation becomes progressively larger with increasing distance from the central region, boosting the effect of the geometric properties h/d_{mean}.

In summary, the observed behavior of the wave velocity results from the complex interplay among multiple factors. As the distance from the heart increases, the stiffening (compliance) of the vessel walls toward the periphery below (above) OIP—together with the geometric variation of vessel wall thickness and inner radius—contributes to the distal increase (decrease) in the propagation speed of the wavefront. This spatial trend of c is essentially preserved under increasing gravitational load. However, gravity induces an additional stiffening effect in the lower-body vessels (or compliance in the upper-body), leading to a general increase (decrease) of wave velocity in that region. In this manner, the human cardiovascular system responds to the enhanced orthostatic load by naturally counteracting venous pooling, with the ultimate goal of preserving central hemodynamic parameters as stable as possible.

C. Traveling waves: Mechanisms of transmission and reflection

Wave decomposition is performed under the water hammer theory,[7,25] as described in Sec. SM3 of the supplementary material. By means of the local characteristic impedance, Z_c, forward and backward pressure and flow rate waves are identified. Examples of forward and backward pressure waves at three representative arterial sites and under four gravitational conditions (0*g*, 1*g*, 2*g, and* 3*g*) are shown in the right panels of Fig. 1, while additional visualizations are offered in Figs. SM4 and SM5 of the supplementary material.

The mean values of the decomposed pressure waves reflect the behavior of the mean total pressures (see Table SM12 in the supplementary material). Both the forward and backward mean pressures exhibit distinct trends under increasing gravitational stress, depending on their position relative to the OIP. Specifically, arterial sites located above heart level (i.e., the carotid arteries) show a reduction in mean pressure values as g increases. Conversely, in the vessels extending from the abdominal aorta to the anterior tibial artery, mean pressure values progressively increase. Moreover, the percentage variation between 0*g and* 3*g* becomes larger with increasing distance from the heart: the abdominal aorta shows a change in forward mean pressure of +42.3%, whereas the anterior tibial artery reaches +241%. Sites located at heart level exhibit minimal variations both in mean forward and backward pressures: the percentage change between 0*g and* 3*g* for the forward/backward signal is −0.92%/+0.79% at the aortic root and −11.30%/−8.12% in the thoracic aorta.

A comparable trend is observed in the mean values of the forward and backward flow rate waves (see Table SM13 in the supplementary material). Arterial sites located above the thoracic aorta exhibit a progressive reduction in mean flow rate with increasing gravitational acceleration. In contrast, vessels in the lower body demonstrate a corresponding increase in mean flow rate under higher g conditions, consistently for both decomposed wave components.

Both the forward and backward pressure waves show a clear decreasing trend in pulse values, from microgravity to hypergravity. This result is consistent with the behavior of the pulse values of total waves, whose reduction is therefore linked to the decreased pulsatility of both decomposed signals. Nevertheless, across all analyzed sites, the backward pulse pressures exhibit a larger percentage reduction compared to their forward counterparts when transitioning from 0*g* to 3*g*. An analogous behavior was observed for the decomposed flow rate waves.

To quantify the gravity-induced pulsatility variations in terms of reflection mechanisms, the reflection parameters RM and RI were computed at all sites of interest over the 0*g*–3*g* gravity range. Figure 3 shows that increasing g along the cranio-caudal axis leads to a remarkable reduction in both RM (panel a) and RI (panel b) at all analyzed locations, irrespective of whether they lie above or below the OIP. Notably, this decrease is also observed in the lower limbs, where the increased hydrostatic load and the higher local characteristic impedance (Z_c) would be expected to enhance wave reflection. Instead, both RM and RI exhibit a monotonic decrease between 0.5*g and* 3*g* at all sites, with the exception of some central vessels that display a slight initial increase between 0*g* and 0.5*g*. A quantitative assessment of the percentage variations further reveals that RI generally undergoes smaller relative changes than RM across gravity levels. The main exception is the internal carotid artery (ICA), where the reductions in the two parameters are nearly identical (−40.4% for RM and −40.0% for RI). Moreover, the ICA exhibits the largest percentage decreases in both indices between 0*g and* 3*g*. In contrast, the thoracic aorta shows the smallest percentage changes for both RM (−16.5%) and RI

23 October 2026 06:47:30

© Author(s) 2026

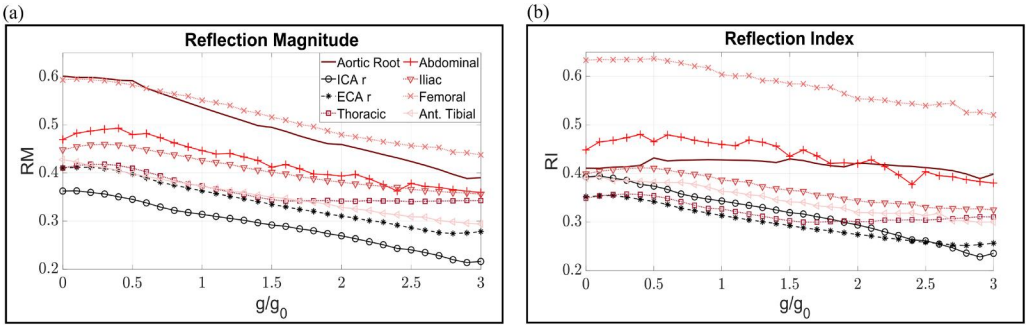

FIG. 3. Wave reflection mechanisms. (a) Reflection magnitude (RM) and (b) reflection index (RI) as function of the gravitational loading at the different arterial sites.

(−11.0%), except for the RI at the aortic root. The latter remains nearly constant across the entire gravity range, decreasing by only −2.9% between 0*g and* 3*g*, compared with a −35.1% reduction in RM at the same site.

Overall, these findings indicate that gravity-induced modifications of pulse pressure and wave reflection are strongly site-dependent. In the ICA, the reflection parameters not only exhibit low absolute values but also the largest relative reductions with increasing gravity. This suggests an enhanced capability of the system to attenuate backward waves relative to both forward and total wave components, consistent with the critical physiological role of the ICA in supplying the cerebral circulation. The close correspondence between ICA RM and RI variations further indicates that forward and total wave amplitudes are modulated similarly across gravity levels. Conversely, central vessels display a distinct behavior between RM and RI. Although the relative variation of the backward wave amplitude with respect to the forward component remains appreciable (as evidenced by the substantial RM changes), its contribution relative to the total wave amplitude is comparatively limited. At the aortic root, this indicates particularly effective attenuation of reflected waves in the vicinity of the aortic valve, a region that is especially sensitive to pressure transients. At the level of the lower limbs, the overall low values of the reflection parameters reveal an unexpected capacity of the arterial network to limit wave reflections, thereby preventing a potentially hazardous increase in backward wave amplitude in response to elevated hydrostatic loading.

RM and RI trends show that gravity alters backward waves more than forward waves. To explain this asymmetry, we decomposed impedance-mismatch effects into bifurcation (R_p), tapering (R_t), and peripheral resistance (r) contributions. Detailed results are offered in Sec. SM7 of the supplementary material (figures from SM9 to SM12), while the key findings across 0*g*–3*g* are summarized as follows:

- Bifurcation reflection coefficient R_p (averaged through the arterial sites) shows strong directional asymmetry: forward wave R_p is about one order of magnitude lower than backward wave R_p, so forward propagation remains preferential while backward waves are largely re-reflected toward the periphery (Table SM15). Because the bifurcation R_p changes little with gravity (Fig. SM9), this mechanism is not the main driver of gravity-dependent differences.
- Although R_t contributes substantially to reflections (being of the same order as the backward wave R_p in the 15 largest vessels), its average value changes little with gravity (Fig. SM10), indicating that vascular tapering is not the primary mechanism of gravity-induced variations.
- Relative to 1*g*, backward wave pulsatility changes more than forward wave pulsatility (larger increase at 0*g* and larger decrease at $g > 1$), yielding non-unitary variation ratios r (Figs. SM11 and SM12). Thus, the effect of distal peripheral resistances, in particular the arterial–arteriolar interface, emerges as the key modulator of reflection across 0*g*–3*g*, which primarily drives forward–backward asymmetry under changing gravity.

D. Wave trapping and reflection horizon effect

To elucidate the interplay between (i) the forward–backward asymmetric behavior of arterial bifurcations and arterial–arterioles interfaces and (ii) the topology of the entire arterial network, it is highly valuable to study transit times of direct (t_{fcw}) and retrograde (t_{back}) wavefronts, as introduced in Sec. II and more in detail described in Sec. SM3 of the supplementary material. Figure 4 shows transit times for different arterial sites and four different gravitational conditions. In each panel, regression lines were fitted for t_{fcw} and t_{back}, yielding distinct linear trends for arterial sites extending from the aortic root to the iliac artery and for those located within the lower limbs. Recall that the difference between t_{back} and t_{fcw} gives the time of reflection *ToR*.

To interpret Fig. 4, we first adopt a spatial reading at fixed *g*: consider an ideal straight pipe with a localized wave source at one end and a rigid distal termination. The forward wavefront would propagate at finite speed, so t_{fcw} would increase with distance from the source, whereas t_{back} would decrease approaching the distal end, implying that *ToR* would decrease to zero. In the arterial network, t_{fcw} still follows the expected behavior, but t_{back} deviates, with nearly parallel fitted trends along the aortic tract and convergence only in the lower limbs. Consequently, *ToR* is almost constant in the aorta and decreases sharply only distally.

The marked departure from the single pipe behavior highlights a key property of the human arterial tree: wave trapping, i.e., the network ability to attenuate distal backward waves so that only reflections generated within a limited effective upstream distance can propagate centrally. A convenient interpretation is to map *ToR* to an equivalent reflection horizon distance, representing the cumulative effect of the downstream network. In a simple pipe, this horizon would coincide with the distal termination, with the equivalent

23 October 2026 06:47:30

© Author(s) 2026

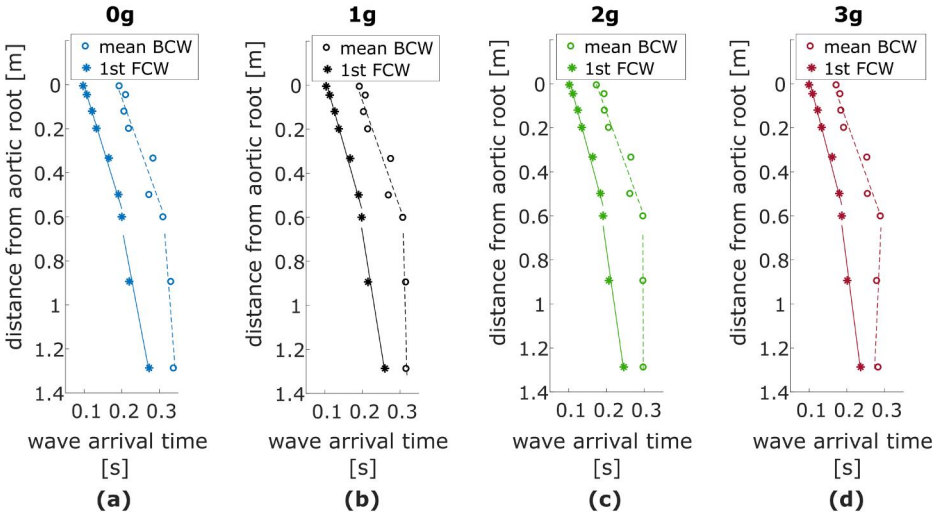

FIG. 4. Analysis of wavefront transit times. Transit times of the forward wavefront (1st FCW) and mean transit times of the backward wavefront (BCW) at nine arterial sites, plotted as a function of the distance from the heart. Results are shown for four gravitational conditions: 0*g* (blue), 1*g* (black), 2*g* (green), and 3*g* (red). For each quantity, two regression lines are reported: one fitted to sites along the aortic and iliac path (vessels 1–44) and one to sites located in the lower limbs (vessels 44–47).

reflection horizon distance maximal at the aortic root and reaching a minimum at the caudal end. In contrast, Fig. 4 shows that, at each gravitational condition, along the aortic tract up to the iliac region the horizon shifts while remaining approximately constant in magnitude, consistent with nearly constant *ToR* and parallel trends of t_{fcw} and t_{back}. Only in the lower limbs, the horizon behaves as in the single pipe limit, yielding progressively smaller *ToR* toward the caudal extremity.

Wave trapping arises from the combined action of local and network scale mechanisms. First, bifurcation geometry attenuates forward reflections and promotes stronger re-reflection of backward components toward peripheral districts (see Table SM15). However, as comparable bifurcation area matching is found along both the aortic tract and lower limbs, local bifurcation geometry alone cannot explain the full phenomenon. A second contribution comes from global arterial topology, i.e., the spatial arrangement of bifurcations and cumulative wave interactions across the network, although the interplay between local geometry and systemic network features remains to be fully clarified. Finally, distal boundary conditions become increasingly important toward terminal regions and, together with the progressive reduction in downstream branching complexity, this explains why wave trapping weakens in the lower limbs toward the periphery.

In the end, focusing on gravity changes, our results show that the response is more pronounced in the return times t_{back}, which progressively decrease with increasing gravitational acceleration. By contrast, the forward wavefront transit times (t_{fcw}) are less affected by variations in *g*, although a slight tendency toward shorter values with increasing distance from the heart is observed at higher gravity accelerations. This behavior results in a progressive decrease in the *ToR* values—and, therefore, a closer reflection horizon—as gravitational acceleration increases (see Table SM16 and Fig. SM13 of the supplementary material).

IV. DISCUSSION AND CONCLUSIONS

The present study provides a model-based analysis of arterial wave transmission under altered gravity, from microgravity to hypergravity (0*g*–3*g*), in standing posture. Increasing gravity shortens the cardiac cycle and reduces pressure and flow pulsatility across the arterial tree, with a clear spatial asymmetry between central and distal regions. The findings highlight two robust trends for wave transmission: at fixed *g*, pulse wave velocity preserves its proximal-to-distal increase, while across gravity levels it decreases above the OIP and increases below it, primarily due to changes in effective wall stiffness rather than vessel geometry alone. Traveling wave decomposition further shows that both forward and backward pulse amplitudes decrease from 0*g* to 3*g*, with stronger attenuation of backward components. Consistently, reflection metrics (*RM* and *RI*) decrease throughout the network, including the lower limbs. Mechanistically, bifurcations and tapering establish directional asymmetry but are only weakly sensitive to gravity, whereas distal peripheral resistances emerge as the main driver of the differential modulation of forward and backward wave amplitudes. Transit time and reflection horizon analyses indicate that wave trapping is preserved: along the aortic tract, reflected wave return times remain consistent with effective filtering of distal reflections, whereas trapping progressively weakens only toward terminal lower limb segments. Overall, the ability to limit the impact of wave reflections along the aortic tract is maintained over a wide range of gravitational loading, from 0*g* to 3*g*.

The present results refer to standing posture, which maximizes the head-to-foot hydrostatic gradient. Sitting and supine configurations should attenuate these gravity-dependent trends, especially in the lower limbs, although thoracic and cardiac effects related to venous return and ventricular filling may persist. Future extensions could assess whether this behavior is preserved under negative-gravity conditions relevant to inverted posture or aerobatic flight and within physiologically constrained, subject-specific model calibrations aimed at personalized cardiovascular predictions and virtual population studies. Moreover, altered-gravity exposure was represented primarily through hydrostatic loading and short-term cardiovascular regulation. Other physiological responses, such as muscle activation, respiratory changes, vestibular and autonomic effects, or longer-term adaptation, were not explicitly modeled and could modulate venous return, ventricular filling, vascular tone, and blood-volume distribution, thereby affecting the predicted wave transmission metrics.

Despite gravity-induced variations in vessel geometric and mechanical properties, a healthy cardiovascular system remains capable

23 October 2026 06:47:30

© Author(s) 2026

of maintaining the wave trapping mechanism. Specifically, the arterial tree inherently protects central systemic vessels from excessive reflected wave content, which could otherwise impair cardiac function and regular forward propagation of pressure and flow waves. From a physical standpoint, pending future clinical confirmation, these findings suggest that the arterial network behaves as a gravity-resilient wave-filtering system, whose geometric organization governs the selective attenuation of reflected waves.

SUPPLEMENTARY MATERIAL

See the supplementary material for details of the cardiovascular model, parameter setting, methodological aspects, and additional results of the waveform analysis.

ACKNOWLEDGMENTS

This study was carried out within the I-2022-05387 project "Optimizing countermeasures against cardiovascular deconditioning and cerebral hemodynamics changes in long-term human spaceflights" (Contract No.: 4000141523) and the I-2025-00714 project "Risk map for the Spaceflight Associated Neuro-ocular Syndrome (SANS) through cardiovascular digital twins" (Contract No.: 4000148742), which were both selected via the Open Space Innovation Platform as Co-Sponsored Research Agreements and carried out under the Discovery Programme of, and funded by, the European Space Agency, France. This manuscript reflects only the authors' views and opinions and the European Space Agency cannot be considered responsible for them.

AUTHOR DECLARATIONS

Conflict of Interest

The authors have no conflicts to disclose.

Author Contributions

S. Scarsoglio: Conceptualization (lead); Formal analysis (lead); Funding acquisition (lead); Methodology (equal); Resources (lead); Supervision (lead); Validation (equal); Writing – original draft (equal); Writing – review & editing (equal). **G. Colussi:** Formal analysis (equal); Methodology (equal); Software (lead); Validation (equal); Visualization (lead); Writing – original draft (equal); Writing – review & editing (equal). **F. Tripoli:** Formal analysis (equal); Methodology (equal); Software (lead); Validation (equal); Visualization (equal); Writing – original draft (supporting); Writing – review & editing (equal). **L. Ridolfi:** Conceptualization (lead); Formal analysis (lead); Methodology (equal); Resources (lead); Supervision (lead); Validation (equal); Writing – original draft (equal); Writing – review & editing (equal).

DATA AVAILABILITY

The data that support the findings of this study are available from the corresponding author upon reasonable request.

REFERENCES

[1]P. Norsk, "Adaptation of the cardiovascular system to weightlessness: Surprises, paradoxes and implications for deep space missions," Acta Physiol. **228**, e13434 (2020).
[2]R. L. Hughson, A. Helm, and M. Durante, "Heart in space: Effects of the extraterrestrial environment on the cardiovascular system," Nat. Rev. Cardiol. **15**, 167–180 (2018).
[3]H. Zhu, H. Wang, and Z. Liu, "Effects of real and simulated weightlessness on the cardiac and peripheral vascular function on humans: A review," Int. J. Occup. Med. Environ. Health **28**, 793–802 (2015).
[4]O. Eiken, M. Keramidas, H. Skoldefors, and R. Kolegard, "Human cardiovascular adaptation to hypergravity," Am. J. Physiol. Regul. Integr. Comp. Physiol. **322**(6), R597–R608 (2022).
[5]F. N. V. de Vosse and N. Stergiopulos, "Pulse wave propagation in the arterial tree," Annu. Rev. Fluid Mech. **43**, 467–499 (2011).
[6]*McDonald's Blood Flow in Arteries: Theoretical, Experimental and Clinical Principles*, 7th ed., edited by W. W. Nichols, M. F. O'Rourke, E. R. Edelman, and C. Vlachopoulos (CRC Press, 2022).
[7]K. H. Parker, "An introduction to wave intensity analysis," Med. Biol. Eng. Comput. **47**(2), 175–188 (2009).
[8]N. Westerhof and B. E. Westerhof, "A review of methods to determine the functional arterial parameters stiffness and resistance," J. Hypertens. **31**(9), 1769–1775 (2013).
[9]J. P. Mynard, A. Kondiboyina, R. Kowalski, M. M. H. Cheung, and J. J. Smolich, "Measurement, analysis and interpretation of pressure/flow waves in blood vessels," Front. Physiol. **11**, 1085 (2020).
[10]N. Westerhof, P. Sipkema, G. V. D. Bos, and G. Elzinga, "Forward and backward waves in the arterial system," Cardiovasc. Res. **6**, 648–656 (1972).
[11]K. H. Parker, C. J. Jones, J. R. Dawson, and D. G. Gibson, "What stops the flow of blood from the heart?," Heart Vessels **4**, 241–245 (1988).
[12]K. H. Parker and C. Jones, "Forward and backward running waves in the arteries: Analysis using the method of characteristics," J. Biomech. Eng. **112**, 322–326 (1990).
[13]N. Westerhof, N. Stergiopulos, M. I. Noble, and B. E. Westerhof, *Snapshots of Hemodynamics: An Aid for Clinical Research and Graduate Education* (Springer, New York, NY, 2010.
[14]P. Boutouyrie *et al.*, "Assessment of pulse wave velocity," Artery Res. **3**, 3–8 (2008).
[15]B. Jiang *et al.*, "Measurement of pulse wave velocity using pulse wave doppler ultrasound: Comparison with arterial tonometry," Ultrasound Med. Biol. **34**(3), 509–512 (2008).
[16]V. Bortel *et al.*, "Expert consensus document on the measurement of aortic stiffness in daily practice using carotid-femoral pulse wave velocity," J. Hypertens. **30**(3), 445–448 (2012).
[17]C. Vlachopoulos *et al.*, "Prediction of cardiovascular events and all-cause mortality with arterial stiffness: A systematic review and meta-analysis," J. Am. Coll. Cardiol. **55**(13), 1318–1327 (2010).
[18]J. E. Davies *et al.*, "Attenuation of wave reflection by wave entrapment creates a 'horizon effect' in the human aorta," Hypertension **60**, 778–785 (2012).
[19]N. Westerhof, P. Segers, and B. E. Westerhof, "Wave separation, wave intensity, the reservoirwave concept, and the instantaneous wave-free ratio: Presumptions and principles," Hypertension **66**, 93–98 (2015).
[20]B. E. Westerhof and N. Westerhof, "Uniform tube models with single reflection site do not explain aortic wave travel and pressure wave shape," Physiol. Meas. **39**, 124006 (2018).
[21]A. Avolio and G. Parati, "Reflecting on posture," J. Hypertens. **29**, 655–657 (2011).
[22]A. Avolio, M. Butlin, and K. Xu, "Reflections on determinants of augmentation index," J. Hypertens. **30**, 267–268 (2012).
[23]W. E. Hughes and D. P. Casey, "Aortic wave reflection during orthostatic challenges: Influence of body position and venous pooling," Am. J. Hypertens. **30**, 166–172 (2017).
[24]A. M. Huijben, F. U. Mattace-Raso, J. Deinum, J. Lenders, and A. H. V. den Meiracker, "Aortic augmentation index and pulse wave velocity in response to head-up tilting: Effect of autonomic failure," J. Hypertens. **30**, 307–314 (2012).
[25]M. Fois, L. Ridolfi, and S. Scarsoglio, "Arterial wave dynamics preservation upon orthostatic stress: A modelling perspective," R. Soc. Open Sci. **10**(3), 221257 (2023).
[26]R. L. Hughson *et al.*, "Increased postflight carotid artery stiffness and inflight insulin resistance resulting from 6-mo spaceflight in male and female astronauts," Am. J. Physiol. Heart Circ. Physiol. **310**(5), H628–H638 (2016).

23 October 2026 06:47:30

© Author(s) 2026

[27]F. Hoffmann *et al.*, "An oscillometric approach in assessing early vascular ageing biomarkers following long-term space flights," Int. J. Cardiol. Hypertens. **2**, 100013 (2019).
[28]A. Krachtis *et al.*, "Arterial stiffness alterations in simulated microgravity and reactive sledge as a countermeasure," High Blood Pressure Cardiovasc. Prev. **29**(1), 65–74 (2022).
[29]P. Boutouyrie *et al.*, "Impact of 60 days of head-down bed rest on large arteries," J. Hypertens. **40**, 2058–2067 (2022).
[30]S. Orter *et al.*, "A comparison between left ventricular ejection time measurement methods during physiological changes induced by simulated microgravity," Exp. Physiol. **107**, 213–221 (2022).
[31]O. Eiken, R. Kolegard, and I. B. Mekjavic, "Pressure-distension relationship in arteries and arterioles in response to 5 wk of horizontal bedrest," Am. J. Physiol. Heart Circ. Physiol. **295**, H1296–H1302 (2008).
[32]C. Palombo *et al.*, "Carotid reservoir pressure decrease after prolonged head down tilt bed rest in young healthy subjects is associated with reduction in left ventricular ejection time and diastolic length," Front. Physiol. **13**, 866045 (2022).
[33]J. M. Lazar *et al.*, "The effects of head-out-of-water immersion on arterial wave reflection in healthy adults," J. Am. Soc. Hypertens. **2**(6), 455–461 (2008).
[34]P. J. Blanco and L. O. Müller, "One-dimensional blood flow modeling in the cardiovascular system. From the conventional physiological setting to real-life hemodynamics," Numer. Methods Biomed. Eng. **41**(3), e70020 (2025).
[35]J. Alastruey *et al.*, "Arterial pulse wave modeling and analysis for vascular-age studies: A review from vascagenet," Am. J. Physiol. Heart Circ. Physiol. **325**(1), H1–H29 (2023).
[36]P. H. Charlton *et al.*, "Modeling arterial pulse waves in healthy aging: A database for in silico evaluation of hemodynamics and pulse wave indexes," Am. J. Physiol. Heart Circ. Physiol. **317**(5), H1062–H1085 (2019).
[37]M. Fois, A. Diaz-Artiles, S. Y. Zaman, L. Ridolfi, and S. Scarsoglio, "Linking cerebral hemodynamics and ocular microgravity-induced alterations through an in silico-in vivo head-down tilt framework," npj Microgravity **10**, 22 (2024).
[38]M. Fois, S. V. Maule, M. Giudici, M. Valente, L. Ridolfi, and S. Scarsoglio, "Cardiovascular response to posture changes: Multiscale modeling and in vivo validation during head-up tilt," Front. Physiol. **13**, 826989 (2022).
[39]F. Tripoli, L. Ridolfi, and S. Scarsoglio, "Short-term response of cerebrovascular and ocular hemodynamics from micro- to hyper-gravity: A multiscale mathematical analysis," Acta Astronaut. **237**, 159–173 (2025).
[40]F. Tripoli, L. Ridolfi, and S. Scarsoglio, "Assessing the cardiac function from micro-gravity to hyper-gravity conditions through a validated multiscale modelling approach," J. Physiol. **604**, 5296 (2026).
[41]C. Gallo, L. Ridolfi, and S. Scarsoglio, "Cardiovascular deconditioning during long-term spaceflight through multiscale modeling," njp Microgravity **6**(1), 27 (2020).
[42]S. Scarsoglio, L. Congiu, and L. Ridolfi, "Investigating the impact of atrial fibrillation on the vascular onset of glaucoma via multiscale cardiovascular modeling," Comput. Methods Programs Biomed. **267**, 108783 (2025).
[43]A. Saglietto, M. Fois, L. Ridolfi, G. M. D. Ferrari, M. Anselmino, and S. Scarsoglio, "A computational analysis of atrial fibrillation effects on coronary perfusion across the different myocardial layers," Sci. Rep. **12**(1), 841 (2022).
[44]S. Scarsoglio, C. Gallo, A. Saglietto, L. Ridolfi, and M. Anselmino, "Impaired coronary blood flow at higher heart rates during atrial fibrillation: Investigation via multiscale modelling," Comput. Methods Programs Biomed. **175**, 95–102 (2019).
[45]S. Scarsoglio, C. Gallo, and L. Ridolfi, "Effects of atrial fibrillation on the arterial fluid dynamics: A modelling perspective," Meccanica **53**(13), 3251–3267 (2018).
[46]V. Guinot, *Wave Propagation in Fluids: Models and Numerical Techniques* (Wiley, 2012).
[47]H. P. Charalambous, P. C. Roussis, and A. E. Giannakopoulos, "The effect of strain hardening on the dynamic response of human artery segments," Open Biomed. Eng. J. **11**, 85–110 (2017).

23 October 2026 06:47:30

© Author(s) 2026